© 2017. Published by The Company of Biologists Ltd | Development (2017) 144, 2381-2391 doi:10.1242/dev.145193

RESEARCH ARTICLE

A new hypothesis for foregut and heart tube formation based on differential growth and actomyosin contraction

Hadi S. Hosseini[1,2], Kara E. Garcia[1] and Larry A. Taber[1,*]

ABSTRACT

For decades, it was commonly thought that the bilateral heart fields in the early embryo fold directly towards the midline, where they meet and fuse to create the primitive heart tube. Recent studies have challenged this view, however, suggesting that the heart fields fold diagonally. As early foregut and heart tube morphogenesis are intimately related, this finding also raises questions concerning the traditional view of foregut formation. Here, we combine experiments on chick embryos with computational modeling to explore a new hypothesis for the physical mechanisms of heart tube and foregut formation. According to our hypothesis, differential anisotropic growth between mesoderm and endoderm drives diagonal folding. Then, active contraction along the anterior intestinal portal generates tension to elongate the foregut and heart tube. We test this hypothesis using biochemical perturbations of cell proliferation and contractility, as well as computational modeling based on nonlinear elasticity theory including growth and contraction. The present results generally support the view that differential growth and actomyosin contraction drive formation of the foregut and heart tube in the early chick embryo.

KEY WORDS: Morphogenesis, Growth, Contraction, Biomechanics, Computational model

INTRODUCTION

Near the anterior end of the early vertebrate embryo, three tubes – the brain tube, the heart tube (HT) and the foregut (FG) – form simultaneously from ectoderm, mesoderm and endoderm, respectively (Patten, 1951). Folding of epithelia creates each of these primitive organs, which begin as relatively straight tubes but later bend and twist to form more complex structures. Because of their proximity in time and space, morphogenesis of these structures is coupled to some extent. This is particularly true for the heart and foregut, which are the focus of this report.

Development of the heart and foregut in the chick embryo is similar to that in mammals, including human (Abu-Issa and Kirby, 2008). These structures are created by folding of the splanchnopleure (SPL), an initially flat bilayered membrane composed of endoderm and splanchnic mesoderm. As folding begins, the presumptive heart fields (HFs) occupy oval-shaped regions of the splanchnic mesoderm on both sides of the embryo (Fig. 1A-A″). Folding inverts the SPL (Fig. 1B′,C′), bringing the two sides of this membrane together at the midline, where the mesodermal and endodermal layers fuse to create the HT and FG, respectively (Fig. 1D-E″). These tubes then elongate as the anterior intestinal portal (AIP), i.e. the opening at the caudal end of the FG, descends (Fig. 1D,D′,E,E′).

For decades, it was commonly thought that the SPL folds in a lateral-to-medial direction, with the SPL maintaining the same cranial-caudal polarity as it creates the HT and FG. During the last 15 years, fate-mapping studies for the heart have challenged this view, however, suggesting that the pattern is more complex (Abu-Issa and Kirby, 2008; Kirby, 2007; Cui et al., 2009). In the new model, the HFs fold diagonally, transforming the initial cranial-caudal polarity to medial-lateral polarity (Fig. 1B′,C′,D′). This process brings the cranial margin of the HFs to the midline, where they fuse to form the ventral side of the HT (future outer curvature of the looped heart). At the same time, the medial aspects of the HFs move cranially to create the outflow portion of the heart (primitive right ventricle), and the lateral aspects move caudally to create the inflow region (primitive left ventricle) (Fig. 1E′). Because the layers of the SPL are adhered, the FG must also be created by this folding pattern.

The physical mechanisms that create the HT and FG remain poorly understood, especially in relation to this revised view of morphogenesis. Here, using a combination of experiments and computational modeling, we examine the plausibility of a new hypothesis for this complex process consisting of three phases: (1) FG formation – differential growth between the splanchnic mesoderm and endoderm, with the mesoderm growing faster, drives SPL folding to create the FG and bring the HFs into their proper orientations at the embryonic midline; (2) AIP descension – after midline fusion, actomyosin contraction along the AIP pulls the SPL downward, causing both layers to stretch longitudinally with SPL growth assisting the elongation; and (3) HT formation – cardiac jelly pressure and circumferential growth, possibly produced by cells entering the HFs from neighboring mesoderm, cause the HFs to expand and create the HT.

RESULTS

The present study focuses on events that take place during Hamburger-Hamilton stages HH5 to HH10 in the chick embryo (Hamburger and Hamilton, 1951). To test our hypothesis experimentally, we inhibited cell proliferation and contraction in cultured embryos. Next, we used computational modeling to determine the physical plausibility of our hypothesis. Finally, we tested the model using additional experimental data.

Foregut and heart tube formation in the chick embryo

To orient readers who may be unfamiliar with this problem, we first describe FG and HT morphogenesis in more detail. For convenience, although there is some overlap, we divide the process into three phases corresponding to the hypothesis described above.

[1]Department of Biomedical Engineering, Washington University, St Louis, MO 63130, USA. [2]Department of Physics, Washington University, St Louis, MO 63130, USA.

*Author for correspondence (lat@wustl.edu)

L.A.T., 0000-0002-6451-8330

Received 28 September 2016; Accepted 10 May 2017

Development (2017) 144, 2381-2391 doi:10.1242/dev.145193

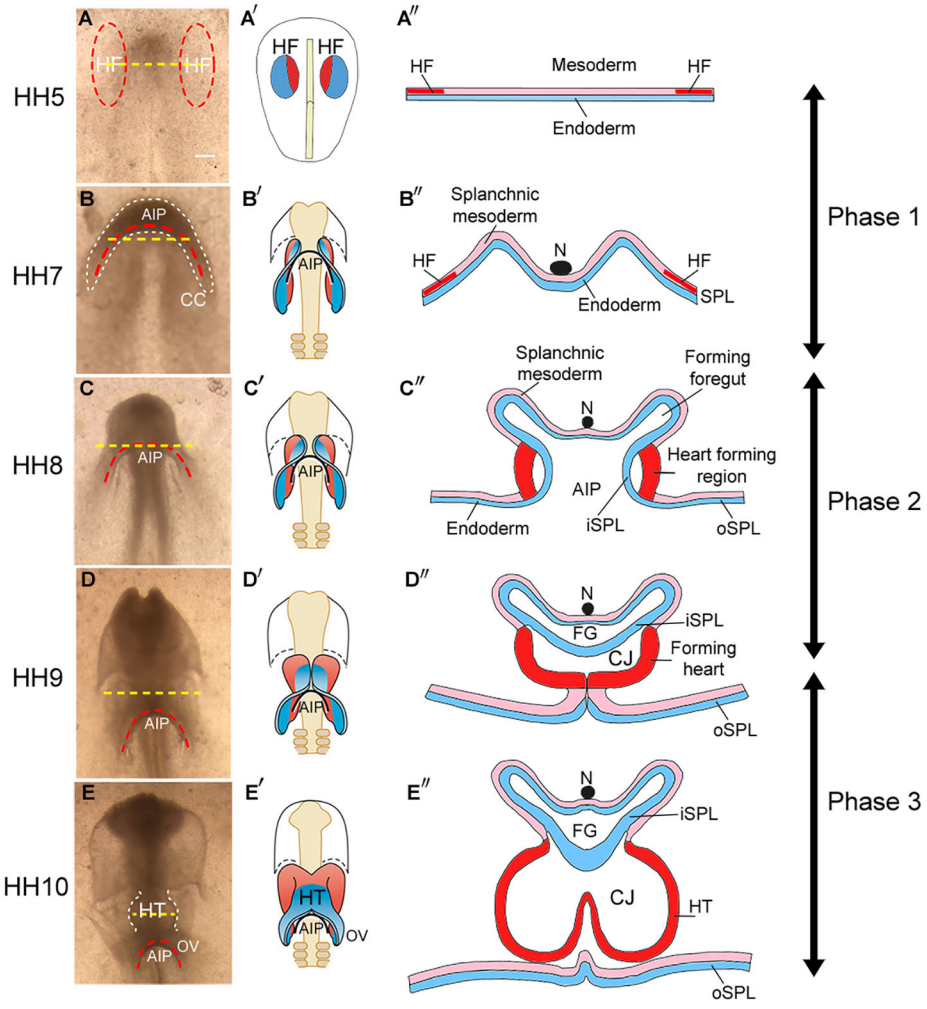

Fig. 1. Morphology of foregut and heart tube formation in chick embryo (stages HH5-HH10). (A-E) Brightfield images of embryo (ventral view). Scale bar: 150 µm (for all images). (A′-E′) Schematics illustrating folding of heart fields (HFs). Lateral regions (blue) and medial regions (red) become inflow and outflow regions of the HT (E′). (A″-E″) Schematics of cross-sections indicated by dashed yellow lines in A-E. Red dashed lines indicate HFs in A and anterior intestinal portal (AIP) in B-E. CC, cardiac crescent; CJ, cardiac jelly; FG, foregut; HT, heart tube; iSPL, oSPL, inner, outer splanchnopleure; N, notochord; OV, omphalomesenteric vein. Schematics in A′-E′ are reprinted, with permission, from Kirby (2007); those in A″-E″ are based on drawings by Kirby (2007).

During the first day of incubation, the tri-layered blastodisc, consisting of ectoderm, mesoderm and endoderm, forms on the surface of the yolk (Patten, 1951). At HH5 (20 h), the HFs are located bilaterally within the mesoderm (Fig. 1A-A″) (Linask and Lash, 1986; DeHaan, 1963; Stalsberg and DeHaan, 1968; Moreno-Rodriguez et al., 2006; Abu-Issa and Kirby, 2007, 2008). By HH7, the mesoderm splits into somatic mesoderm, which is connected to ectoderm on the dorsal side of the embryo, and splanchnic mesoderm, which contains the HFs and is attached to endoderm on the ventral side (Fig. 1B″). The splanchnic mesoderm and endoderm together make up the SPL. We define two regions of SPL on each side of the embryo: (1) inner SPL (iSPL), destined to create the FG and HT; and (2) outer SPL (oSPL), destined to form a membrane outside the FG on the ventral side of the HT (Fig. 1C″-E″).

Phase 1: Foregut formation (HH5-7)

After the pre-cardiac cells epithelialize, the SPL (including HFs) starts to fold (Fig. 1B-B″) (Kirby, 2007). Except for a small relative motion, the two layers of the SPL move together (Abu-Issa, 2014; Aleksandrova et al., 2015), suggesting that they fold as a contiguous sheet. The left and right sides of the iSPL fold diagonally towards the midline, where their originally cranial margins meet and fuse gradually from top to bottom. This motion inverts the iSPL while simultaneously carrying the medial regions of the HFs (red) cranially and the lateral regions (blue) caudally (Fig. 1B′-D′), thereby creating the early FG, a tube open at the AIP, while moving the HFs into their proper orientation for HT formation (Kirby, 2007).

Phase 2: AIP descension (HH7-9)

Both the iSPL and the oSPL lengthen axially as the AIP moves downward. This process also lengthens the FG and the fused HFs, which begin to separate from the endoderm (Fig. 1C-D″) (Linask and Lash, 1986; Schultheiss et al., 1995).

Phase 3: Heart tube formation (HH9-10)

The fused HFs thicken and expand to create the HT (Fig. 1D″,E″). By stage HH10 (33 h), the HT is a relatively straight, tapered tube that is open and connected to the FG along its dorsal side (Fig. 1E-E″; see also Fig. 7A). The unfused regions of mesoderm at the caudal end of the HT form the omphalomesenteric veins (Fig. 1E′). Accumulating extracellular matrix (cardiac jelly) separates the expanding mesoderm (myocardium) from the endoderm (Fig. 1E″) (Romanoff, 1960).

Cell proliferation is required for foregut morphogenesis

To examine the effects of cell proliferation during Phase 1, we cultured HH5 embryos in media containing the mitotic inhibitor aphidicolin (50 µM). Staining with EdU (5-ethynyl-2′-deoxyuridine) confirmed the effectiveness of aphidicolin (Fig. S1). Compared with control embryos (n=5), little or no folding occurred in treated

Development (2017) 144, 2381-2391 doi:10.1242/dev.145193

embryos (n=4) during the first 5 h of incubation (Fig. 2A,B). After the drug was washed out, relatively normal folding and AIP descension occurred (Fig. 2B), creating a partially looped HT after an additional 25 h of culture. Development was delayed, however, and the HT had an abnormal shape and relatively weak heartbeat (Fig. 2B). In treated embryos without washout, folding was inhibited during the entire 30-h culture period (data not shown).

To examine the effects of blocking proliferation during Phases 2 and 3, we cultured HH8 embryos for 21 h in 50 µM aphidicolin. Compared with control embryos (n=4), AIP descension was slower in treated embryos (n=7) during 8 h of incubation, as shown by measurements of relative oSPL length (Fig. 2C). After 21 h of incubation, two beating HTs had formed in most embryos (n=3/4) (Fig. 2C, red dashed lines). Exposure beginning at HH9 yielded similar results (not shown).

Taken together, these results suggest that cell proliferation is required during Phase 1 for the initial folding of the iSPL. Inhibiting proliferation during Phase 2 impedes but does not block iSPL elongation and AIP descension. Thus, consistent with our hypothesis, cell proliferation is required for FG morphogenesis during both Phases 1 and 2. However, our data are inconclusive on the importance of proliferation in HT expansion during Phase 3.

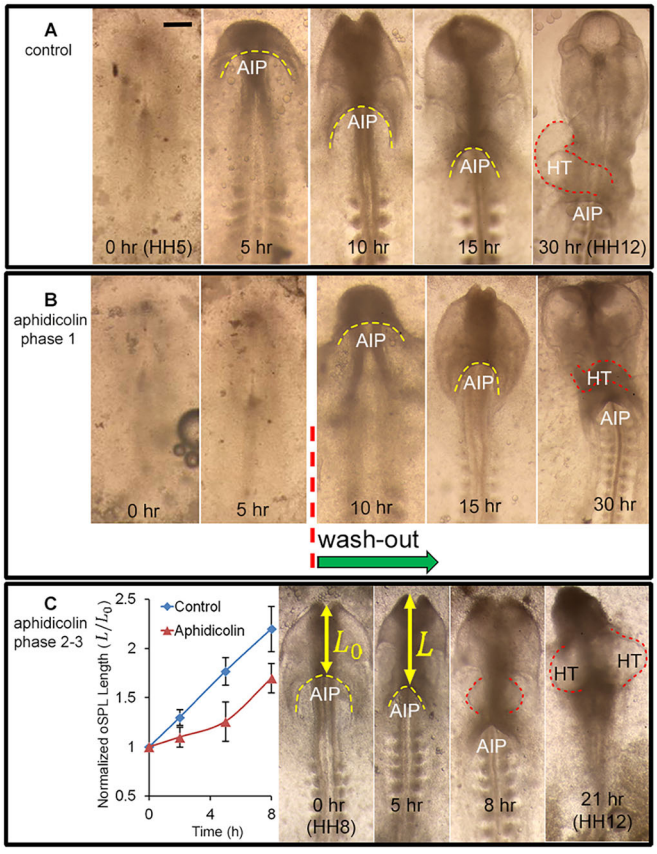

Fig. 2. Effects of inhibiting cell proliferation. (A) Representative chick embryo cultured in normal media for 30 h from stage HH5 (ventral view). Folding of the splanchnopleura (SPL) creates the foregut as the anterior intestinal portal (AIP, yellow dashed line) descends progressively. After 30 h, the heart tube (HT; red dashed line) is looped towards the right. Scale bar: 250 µm. (B) Embryo cultured for 5 h in media containing the mitotic inhibitor aphidicolin (50 µM) shows negligible folding. After washout and continued culture, folding and AIP descension began. At the end of the incubation period, an abnormal HT had formed. (C) Embryo cultured in media containing aphidicolin (50 µM) for 21 h from stage HH8. Plot of relative oSPL length L/L_0 (mean±s.d.) shows that exposure to aphidicolin (n=7) decreased the rate of AIP descension relative to controls (n=4). For this embryo, the treatment resulted in the formation of two heart tubes (HT, right). These results suggest that inhibiting cell proliferation blocks initial folding of the SPL and slows downward motion of the AIP at later stages.

AIP descension requires actomyosin contraction

To determine the effects of actomyosin contraction, we cultured HH5 embryos in media containing the myosin inhibitor blebbistatin (75 µM). During the first 7.5 h of incubation, folding of the iSPL occurred in treated embryos (n=4; Fig. 3Aa-Ad), but AIP descension proceeded at a progressively slower rate (Fig. 3B). After 7.5 h, blebbistatin was washed out and culture continued for an additional 7.5 h (Fig. 3Ae-Ah). After washout, AIP descension resumed and approached the normal rate (Fig. 3B), leading to the formation of an HT (Fig. 3Ah). These results suggest that contraction is not needed for folding of the iSPL during Phase 1 or for HT formation during Phase 3, but it is required for normal AIP descension and the accompanying FG and HF elongation during Phase 2.

The results from these blebbistatin experiments support our hypothesis for Phases 1 and 2. However, as blebbistatin inhibits cytokinesis, it may seem that these experiments contradict our hypothesis for Phase 3, which requires growth for HT formation. On the other hand, stem cell-derived cardiomyocytes can undergo mitosis and form larger cells with two nuclei when treated with blebbistatin (Li et al., 1997; Földes et al., 2011). To determine how blebbistatin affects growth in the chick embryo during the studied stages, we estimated growth strains. The results indicate that blebbistatin exposure slows but does not stop growth in the FG (Fig. 4). If both layers of the SPL are affected similarly, the differential growth between layers that drives folding would be maintained.

Computational model captures FG and HT morphology

To examine the biomechanical feasibility of our hypothesis, we used computational modeling. During Phases 1 and 2, our finite-element model includes only the iSPL, which is treated as a pseudoelastic plate composed of two layers representing endoderm and (splanchnic) mesoderm (Fig. 5A). In the initial configuration (stage HH5), the width, length and thickness of the plate are a=650 µm, b=1900 µm and h=14 µm, respectively, and both layers have the same thickness. Because of bilateral symmetry, the model represents the iSPL on only one side of the embryonic midline (y-axis), with appropriate symmetry conditions applied during the simulation. The boundaries along the x- and y-axes are constrained by roller supports to move only along these axes (Fig. 5B,C).

The boundary conditions along the other two edges of the iSPL require some explanation. During Phases 1 and 2 we assume that the oSPL relaxes or grows to accommodate the motions of the iSPL. Otherwise, the connections between these regions would inhibit iSPL folding. Therefore, although this assumption warrants future study, we take these edges as free of loads and constraints. On the other hand, experimental evidence suggests that the oSPL contracts and stiffens later and plays a role in torsion of the HT during looping (Voronov et al., 2004). Thus, the oSPL is included during Phase 3 as a flat plate with fixed edges positioned near the ventral surface of the HT (see HH10 cross-section in Fig. 6).

The HF is represented by a rectangular region located at the cranial-lateral corner of the mesoderm (Fig. 5B, red). (The shape and location are rough approximations for the actual HF.) The prospective AIP border region is defined as a thin band along the lateral edge of the endoderm (Fig. 5C, green). The layers are bound together except for the HF region, where frictionless contact allows

Development (2017) 144, 2381-2391 doi:10.1242/dev.145193

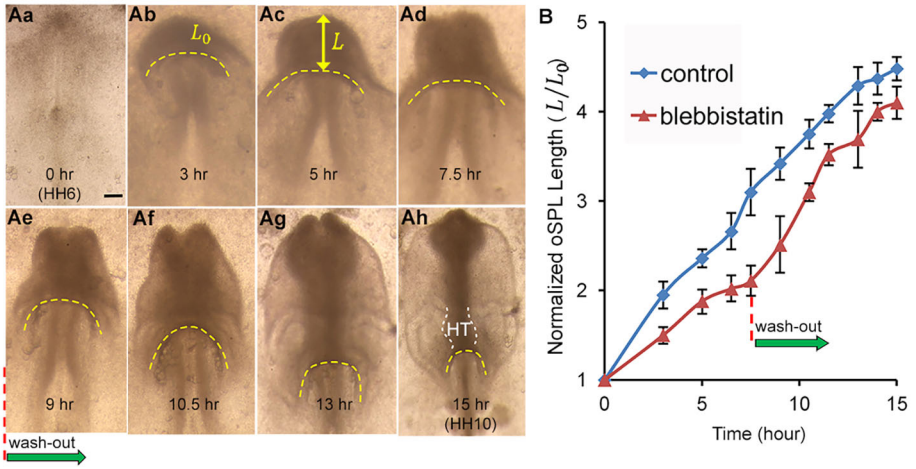

Fig. 3. Effects of inhibiting contraction. (Aa-Ah) Representative chick embryo cultured for 15 h from stage HH6 (ventral view). Yellow dashed lines indicate anterior intestinal portal (AIP). (Aa-Ad) Embryo cultured for 7.5 h to HH7+ in media containing the myosin inhibitor blebbistatin (75 µM). Initial folding of splanchnopleure (SPL) occurred, but after 5 h downward movement of the AIP slowed to nearly a stop. (Ae-Ah) After washout at 7.5 h, AIP descension resumed as heart tube (HT) formed (dashed white lines). (B) Normalized length of oSPL (L/L_0; mean±s.d.) as a function of incubation time for control embryos (n=4) and blebbistatin-treated embryos (n=4). AIP descension rate slowed until washout, then returned to approximately normal. These results suggest that, after initial folding, contraction is required for normal elongation of the SPL and downward motion of the AIP. Scale bar: 150 µm.

relative motion between layers. This lets the layers separate at later stages to create the HT.

The following paragraphs describe the simulation and results for each phase. As described in supplementary Materials and Methods, growth and contraction are simulated by specifying changes in the local zero-stress configuration for each material element (Rodriguez et al., 1994; Taber, 2009).

Phase 1: Foregut formation

The hypothesis for Phase 1 (t=0-4 h; times are defined relative to stage HH5) is based partly on findings by Bellairs (1955) and Miller et al. (1999), who found patterns of cell proliferation in the endoderm of chick embryos that correlate with the folding that creates the foregut. From these data and our aphidicolin results, we speculate that a distinct pattern of growth in the mesoderm and endoderm, with differences in the x and y directions, is necessary to generate diagonal folding of the iSPL. In addition, bending of the iSPL with endoderm located at the inner curvature requires the mesoderm to grow faster than the endoderm, consistent with measurements of Bellairs (1957) and Miller et al. (1999). The relatively rapid proliferation of mesodermal cells on the FG floor (ventral side) is also consistent with the idea that these cells later enter the growing HT (van den Berg et al., 2009).

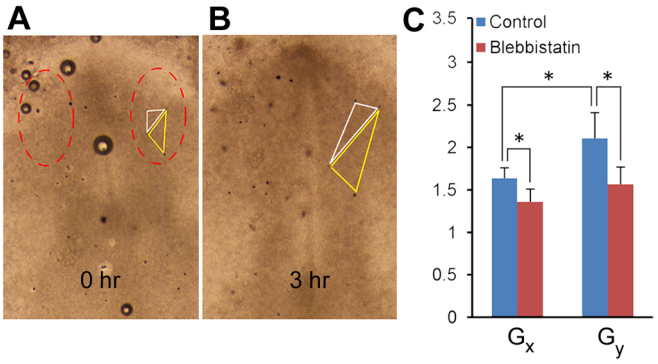

Fig. 4. Effects of blebbistatin exposure on growth of the SPL during Phase 1. (A,B) Embryo with attached beads at HH5 and after 3 h of culture. Two representative triangles used to compute tissue strains are indicated. Analyzed beads were taken from the regions marked by red ovals. (C) Growth ratios G_x and G_y computed from strain and stress data (see supplementary Materials and Methods). Results are shown for control embryos (n=8) and blebbistatin-treated embryos (n=7) (two-way ANOVA, *P<0.01). Blebbistatin exposure slowed but did not stop growth in both the x and y directions.

When these growth patterns are specified in our model (Fig. 5D; see Eqn S6), the iSPL folds diagonally, as observed experimentally, producing morphology in reasonable agreement with experiments (Fig. 6). Folding during Phase 1 is complete at HH7 when the originally upper edge of the iSPL aligns with the midline. Midline fusion of the iSPL with its mirror image on the other side is simulated by changing the free boundary conditions along this edge to roller supports to prevent further lateral displacement.

Phase 2: AIP descension

According to our hypothesis for Phase 2 and consistent with experimental and modeling studies of Aleksandrova et al. (2015), contraction near the arch-shaped AIP generates tension that pulls the AIP downward. Contraction is simulated in our model by specifying negative growth (shortening) tangential to the AIP within the relatively thin region of endoderm representing the AIP border (Fig. 5C, green region). In addition, we include positive axial growth in the iSPL, consistent with experiments suggesting that growth occurs in the floor of the foregut as the AIP descends (Kirby et al., 2003).

When these mechanisms are turned on, the AIP descends as the iSPL elongates, similar to the behavior that occurs in the embryo (compare Fig. 1A and Fig. 6, top row, Phase 2). In addition, the HF in the mesoderm begins to separate from the endoderm (Fig. 6, cross-sections, HH8-9). These shape changes are generally consistent with observed morphology, although the cross-section of the FG in the model is not as flattened as that seen in the chick embryo during this phase.

Phase 3: Heart tube formation

Relatively little cell proliferation occurs in the forming heart during stages HH8-10. However, the HT can grow by addition of proliferating cells from neighboring splanchnic mesoderm (van den Berg et al., 2009). This growth is simulated during Phase 3 in an average sense by specifying circumferential and radial growth in the HF as functions of time. Circumferential growth causes the HF to expand, creating the primitive HT, while radial growth increases the thickness of the heart wall (Fig. 6, middle row).

Two additional features affect the shape of the HT. First, cardiac jelly accumulates and swells inside the HT, forcing the myocardium to expand (Nakamura and Manasek, 1978, 1981). Exposure of stage HH8 embryos to hyaluronidase confirmed that cardiac jelly is necessary for this behavior during Phase 3 (Fig. S2). Thus, cardiac jelly pressure is included in the model by specifying pressure

Development (2017) 144, 2381-2391 doi:10.1242/dev.145193

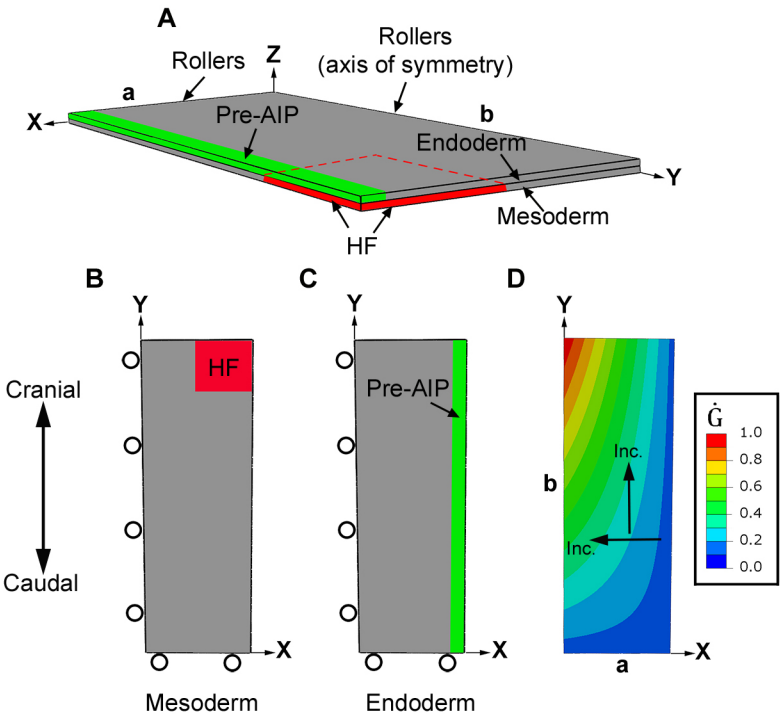

Fig. 5. Finite-element model for foregut and heart tube formation in initial configuration (HH5). (A) The model for the inner splanchnopleure (iSPL) is a flat plate consisting of two layers representing the mesoderm and endoderm. Because of bilateral symmetry, only half of the iSPL is modeled with the *y*-axis representing the embryonic midline. Roller boundary conditions are indicated; other surfaces are free. (B,C) Ventral views of mesoderm and endoderm layers. Black circles indicate roller boundary conditions. Red and green denote regions representing the heart field (HF) and presumptive anterior intestinal portal (AIP), respectively. (D) The spatial pattern of growth rate ($\dot{G} = (1 - \bar{X})\bar{Y}$, see Eqn S6) is the same for both layers during Phase 1, when diagonal folding of iSPL occurs. Growth rate is normalized to the maximum rate in each layer, but actual growth rates are higher in mesoderm (see supplementary Materials and Methods). Arrows indicate directions of increasing (Inc.) growth rate.

between the separating endoderm and HF (Manasek et al., 1984). Second, ventral contact with the oSPL, represented by a separate membrane during Phase 3, further modifies HT shape (Fig. 6, middle row, right). With these effects included, the cross-sectional shape of the HT agrees reasonably well with that in the embryo at HH10, and the FG acquires a shape closer to its characteristic morphology (Fig. 6, HH10). Including cardiac jelly pressure makes the HT slightly rounder (Fig. S4B,B′). In addition, consistent with experimental observations, the HT begins to close on its dorsal side where it is attached to the FG (Fig. 6, middle row, HH9-10).

To evaluate the predicted cardiac morphology in more detail, we compare ventral and cross-sectional shapes between model and experiment at HH10 (Fig. 7). In our model, the omphalomesenteric veins (OVs) correspond to the regions around the AIP below the HT (Fig. 7B). The shapes of the HT and OVs produced by the model are reasonably accurate, although the OVs are too narrow because of simplified constraints at the caudal edge of the iSPL. Cross-sectional shapes along the embryonic axis also are reasonable, although, as already mentioned, the FG is not as flat as that observed *in ovo* (Fig. 7C,D). Part of this discrepancy in FG shape can be

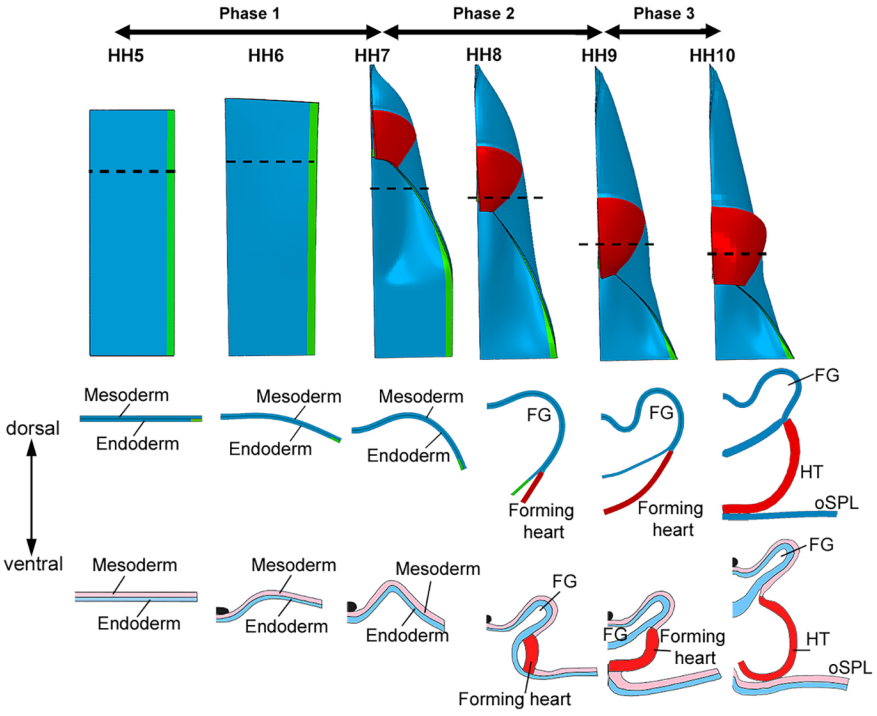

Fig. 6. Results from computational model for folding of inner splanchnopleure (iSPL). Top row: Ventral view of the model at stages HH5-10, divided into three phases. Phase 1: differential growth between SPL layers; Phase 2: contraction along anterior intestinal portal (AIP, green); Phase 3: growth of heart field (HF, red). Middle row: Cross-sections from the model at locations indicated by the dashed black lines. Bottom row: Schematics of the same cross-sections [based on drawings from Kirby (2007)]. Although there are some morphological differences, the model captures the evolving shapes of the foregut (FG) and heart tube (HT) reasonably well.

Development (2017) 144, 2381-2391 doi:10.1242/dev.145193

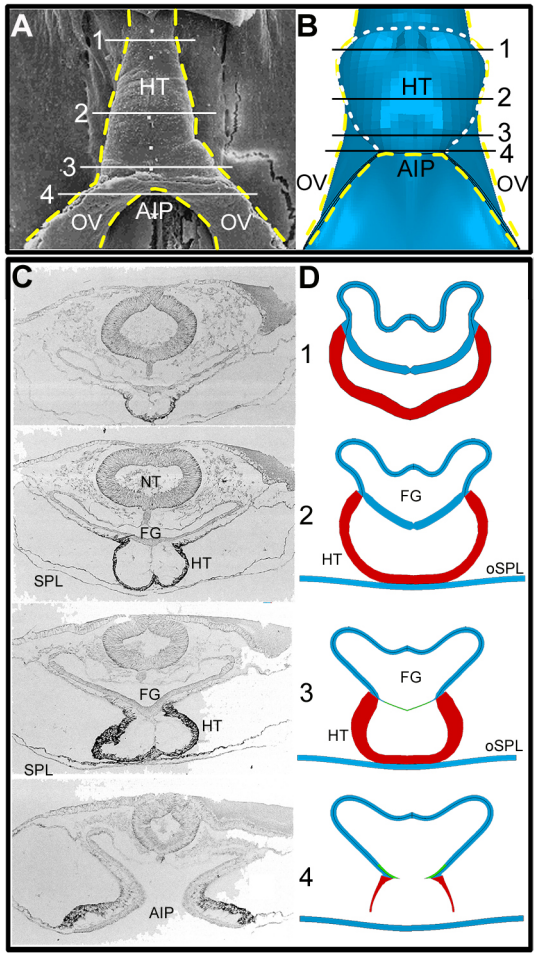

Fig. 7. Comparison of HH10 heart shapes: experiment and model (ventral view). (A) Scanning electron microscopy image [reproduced, with permission, from Männer (2000)]. (B) Model at HH10. Modeled half of embryo is combined with its mirror image to aid visualization. Yellow dashed lines represent outline of heart tube (HT) and omphalomesenteric veins (OVs); white dashed line in B indicates fused heart-field region in the model. OVs represent posterior regions of inner splanchnopleure (iSPL) that have not yet fused. (C,D) Transverse cross-sections of HH10 chick embryo and model at locations indicated by white/black lines in A and B, respectively. Thin green lines in model sections 3 and 4 are the contracting AIP border region. [Experimental sections are reproduced, with permission, from De Jong et al. (1990).] AIP, anterior intestinal portal; FG, foregut; NT, neural tube.

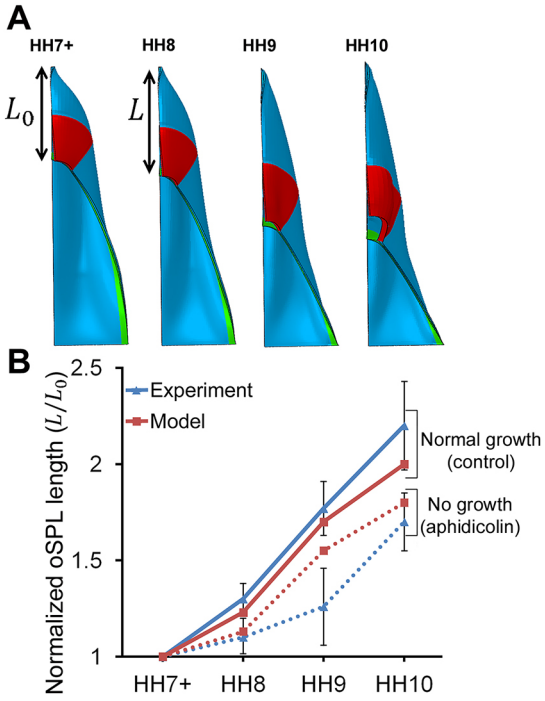

Fig. 8. Simulation of growth inhibition experiment. (A) Ventral view of model during stages HH7+ to HH10 with growth turned off. Green and red regions represent anterior intestinal portal region and heart field, respectively. Compare with model for control embryo in Fig. 6. (B) Plot of normalized oSPL length (L/L_0) versus stage. Experimental results for control embryos (n=4) and embryos exposed to aphidicolin (n=7, mean±s.d.; beginning at HH7+) are compared with model predictions for normal growth and no growth, respectively.

attributed to neglecting the constraints of the neural tube and surrounding mesenchyme in our model.

Taken together, all these results generally support the plausibility of our hypothesis for early FG and HT formation (see Movies 1 and 2).

Model is consistent with other data

Determining physical mechanisms for morphogenesis is complicated by the possibility that multiple mechanisms can produce similar shapes (Varner and Taber, 2012b). Hence, it is important to test models using other data. In addition to morphology, we examine the ability of our model to capture results given by pharmacological perturbations, as well as measures of deformation and stress.

Growth and contraction inhibition

Experimental inhibition of cell proliferation prevented SPL folding during Phase 1 and slowed AIP descension during Phase 2 (n=7; Fig. 2). Our model is consistent with the first result, as initial folding is driven entirely by growth. To examine the second result, we ran the model to HH7+ and then turned off all growth while AIP contraction continued unabated (Fig. 8A). In the model, axial growth normally relieves tension in the iSPL as the AIP is pulled downward. Without this growth, the increased iSPL tension resists this motion, slowing AIP descension, as observed in aphidicolin-treated embryos (Fig. 8B).

Exposure to the myosin inhibitor blebbistatin had relatively little effect on SPL folding during Phase 1, but slowed and eventually stopped AIP descension during Phase 2 (n=4; Fig. 3). Our model is consistent with these results, as it includes no contraction during Phase 1, but contraction supplies the main force that pulls the AIP downward during Phase 2.

Deformation

At selected time points from HH7 to HH9, the motions of embedded beads were used to compute the tangential deformation rate D_T along the AIP during Phase 2 (n=11; Fig. 9A,B). Data from Ramasubramanian et al. (2006), who used the same technique, are included for Phase 3 (Fig. 9C). Negative D_T indicates that the tissue around the AIP shortens. In interpreting these results, it is important to note that D_T is the total deformation rate, which comprises elastic deformation, contraction and growth.

The experimental shortening rate (magnitude of D_T) increased from HH7 to HH8+ and then decreased afterwards. The trends given by the model are strikingly similar (Fig. 9C). Notably, the rate decreases from HH8+ to HH9 even though the strength of

Development (2017) 144, 2381-2391 doi:10.1242/dev.145193

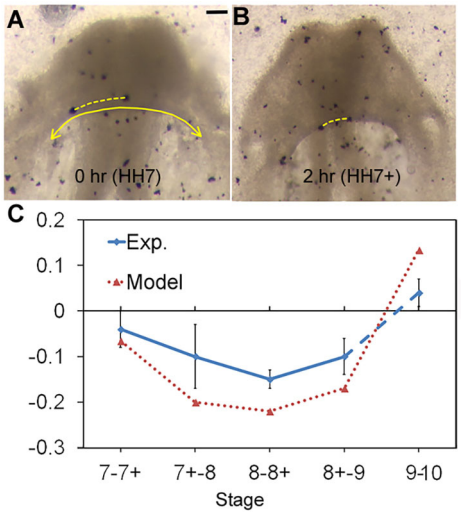

Fig. 9. Deformation rate around AIP during heart tube formation. (A) Tungsten beads (black dots) were injected into an embryo at HH7 (ventral view). Scale bar: 100 µm. (B) The same embryo after 2 h of culture. Dashed yellow curves show a representative pair of beads used for calculations. (C) Comparison of experimental (n=11) and model-predicted deformation rate averaged over the region indicated by arrows in A. For experiments, mean±s.d. are plotted versus stage. Deformation rate D_T was computed tangent to the AIP in the current configuration. Blue dashed line indicates results computed from data given in Ramasubramanian et al. (2006).

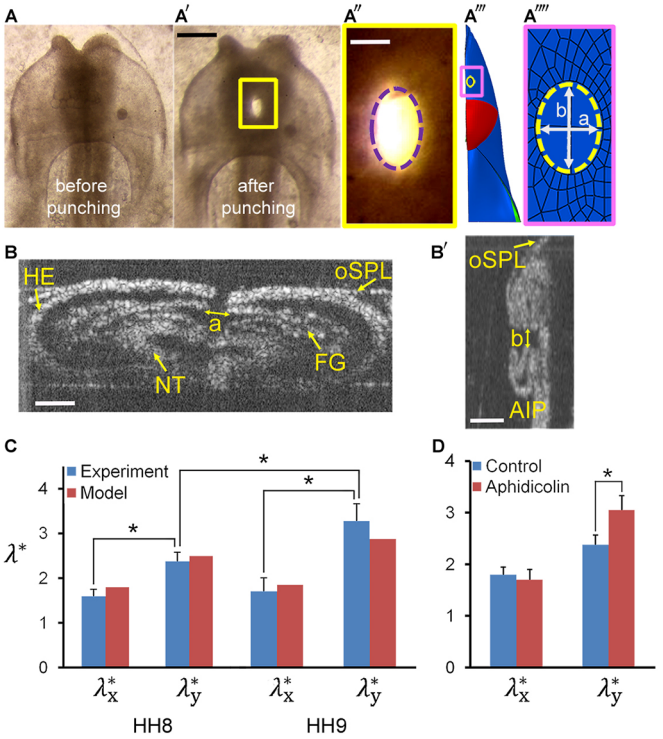

Fig. 10. Tension in foregut. (A,A′) Representative HH8 embryo immediately before and after punching a circular hole (ventral view). (A″) Ellipse (dashed line) was fit to the wound opening (expanded view of yellow box in A′). (A‴) Finite-element model at HH8 with circular hole in inner splanchnopleure (iSPL) introduced at HH5. (A⁗) Ellipse was fit to the model wound opening (expanded view of pink box in A‴). (B,B′) OCT images of transverse and longitudinal cross-sections, respectively, for the embryo shown in A′. A pipette was used to punch holes though oSPL, head ectoderm (HE) and foregut (FG, iSPL). Lengths a and b correspond to minor and major axes of elliptical wound in FG floor. (C) Experimental and model-predicted results for elastic stretch ratios ($\lambda_x^* = a/d$, $\lambda_y^* = b/d$; d=pipette diameter) at stages HH8 (n=6) and HH9 (n=5) (two-way ANOVA, *P<0.01). (D) Experimental elastic stretch ratios in the FG for stage HH8+ embryos cultured from stage HH8 onwards in control media (n=7) and media containing 50 µM aphidicolin (n=8). Inhibition of cell proliferation resulted in increased FG tension in the axial direction during Phase 2 (two-way ANOVA, *P<0.01). AIP, anterior intestinal portal; NT, neural tube. Scale bars: 50 µm (A″); 100 µm (B); 200 µm (A′,B′).

actomyosin contraction continues to increase (growth rate Gy decreases in the AIP region). This behavior is caused in part by increasing tension in the AIP, which produces elastic stretching that partially offsets contraction. Circumferential growth of the HT during Phase 3 leads to a net expansion of the AIP by HH10 (Fig. 9C).

Stress

Tissue stress was characterized by cutting the tissue and immediately measuring the resulting deformation. The amount that the cut opens reflects the magnitude of the tension.

For the FG, we punched circular holes through the oSPL of stage HH8 (n=6) and HH9 (n=5) embryos. The wounds opened into elliptical shapes (Fig. 10A′,A″), and sections acquired by optical coherence tomography (OCT) reveal that the wounds penetrated the oSPL and head ectoderm, as well as the FG (Fig. 10B,B′). As described in Materials and Methods, transverse (λ_x^*) and axial (λ_y^*) elastic stretch ratios in the FG were estimated from measurements of wound geometry in OCT images. The stretch ratios characterize stresses in the corresponding directions, with $\lambda_x^*, \lambda_y^* > 1$ indicating tension (Varner and Taber, 2009). Similar cuts were simulated in the model (Fig. 10A‴,A⁗).

The wounds were consistently elongated in the axial direction, indicating relatively higher tension axially than transversely. The data suggest that axial tension ($\sim\lambda_y^*$) increases significantly from HH8 to HH9 (Phase 2), but transverse tension changes relatively little (Fig. 10C). The results given by the model agree well with these data. In addition, aphidicolin exposure causes the axial tension to increase even more during Phase 2 (Fig. 10D), consistent with our model and supporting the view that growth helps reduce iSPL tension as the AIP descends.

Varner and Taber (2012a) and Shi et al. (2015) used linear incisions to examine tension in the AIP during stages HH8-10 (Fig. 11A). We simulated these experiments by running the model to the appropriate stage and then freeing a segment at the center of the AIP (Fig. 11A′). Comparing experimental and model-predicted opening angles shows relatively good agreement across stages (Fig. 11A″). Similar data for the HT are provided by Shi et al. (2014). For this case, the model includes a cut in the initial geometry, and the opening angle was measured at the end of the simulation. Although some wrinkles appeared in the model because of the cut, results from the model agree reasonably well with the experimental measurements (Fig. 11B-B‴).

Taken together, these additional tests of the model support the plausibility of our hypothesis.

DISCUSSION

For decades, researchers have suggested that HT and FG morphogenesis are interrelated in the early embryo, because both tube-like structures form at essentially the same place and time (Patten, 1951). However, although much is now known about the genetic and molecular factors involved in heart development (Kirby, 2007; Yutzey and Kirby, 2002; Olson and Srivastava, 2002), the physical forces that create and shape both the heart and the foregut remain incompletely understood.

Development (2017) 144, 2381-2391 doi:10.1242/dev.145193

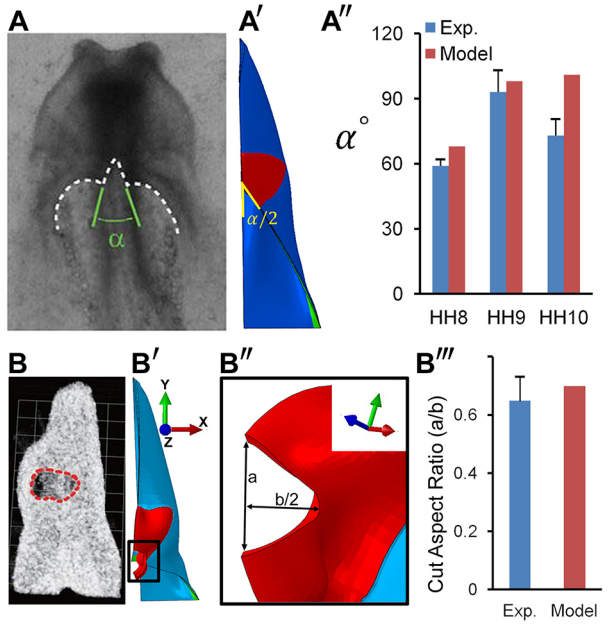

Fig. 11. Tension in anterior intestinal portal (AIP) and heart tube (HT). (A) HH8 embryo immediately after a linear cut at the medial point of the AIP. White dashed curve outlines AIP with cut. [Reproduced, with permission, from Varner and Taber (2012a).] The opening angle α characterizes the magnitude of tension tangential to AIP. (A′) Finite-element model for an AIP cut at HH8. (A″) Comparison of experimental (mean±s.d.) and model results at different stages of development. Experimental data for stage HH8 are reproduced, with permission, from Varner and Taber (2012a); data for stages HH9 and HH10 are reproduced, with permission, from Shi et al. (2014). (B) HH10 heart with circumferential cut. Cut opens to indicate longitudinal tension (dashed ellipse) [reproduced, with permission, from Shi et al. (2014)]. (B′) Model at HH10 with horizontal cut in heart. (B″) Enlarged view of the black box in B′. (B‴) Experimental (n=6) and model-predicted results for cut aspect ratio (a/b). Experimental data are from Shi et al. (2014).

Early work on FG development focused on describing folding morphology. From cross-sectional images and marking experiments, Bellairs (1953a,b) concluded that the left and right sides of the SPL fold directly towards the midline, where they progressively fuse in the cranial-to-caudal direction, lengthening the FG as the AIP moves downward. Because the layers of the SPL are connected by extracellular matrix (Aleksandrova et al., 2015), Bellairs (1953a,b) also suggested that folding of the endoderm carries pre-cardiac mesoderm into its correct position. Recent studies have confirmed this important role for the endoderm, showing that the two layers move together except for relatively small motions of pre-cardiac cells relative to the endoderm (Varner and Taber, 2012a; Aleksandrova et al., 2015).

Focusing on the heart, Stalsberg and DeHaan (1969) described how the bilateral HFs invert to create the HT, suggesting that the HFs also fold directly towards the midline and fuse like the FG. This ‘traditional view’ of HT formation was widely accepted for several decades until the studies of Abu-Issa and Kirby (2007, 2008), who concluded that the HFs fold diagonally rather than straight towards the midline. Although the possible relation to endodermal motion was mentioned (Abu-Issa, 2014), these investigators apparently did not attempt to relate morphogenesis of the HT to that of the FG.

These new results for the HT suggest that the traditional view of FG formation also should be re-examined. In the present study, therefore, we have proposed and tested a new mechanistic hypothesis that integrates HT and FG morphogenesis. Aspects of our hypothesis build on previous work by Aleksandrova et al. (2015), who used *in vivo* imaging and computational modeling to study HT formation.

Phase 1: Foregut formation

Results from our model show that the folding pattern of the HFs described by Abu-Issa and Kirby (2007, 2008) can be produced by orthotropic growth (in the x and y directions) of both layers of the iSPL, with the mesoderm growing more rapidly. This growth pattern also creates an endoderm-lined FG and an arch-shaped AIP (Fig. 6). A growth-driven mechanism for iSPL folding is supported by our experiments in which inhibiting cell proliferation blocked the initial folding (Fig. 2B).

Growth of splanchnic mesoderm alone could give similar results, but cells proliferate in the FG-forming region of the chick endoderm during these stages (Bellairs, 1955; Miller et al., 1999) (Fig. S1). Similar behavior also could be produced by contraction of the endoderm, but this possibility is inconsistent with our experiments showing that folding during Phase 1 occurs when actomyosin contraction is inhibited (Fig. 3Aa-Ad). Because differential growth and contraction are the two most common mechanisms for epithelial bending in the embryo (Davies, 2005; Taber, 2014), including the growth that bends the looping HT (Shi et al., 2014), we conclude that folding of the iSPL is driven primarily by differential growth between the layers.

Published data generally support the spatial patterns of cell proliferation in our model. In the endoderm, Bellairs (1955) found a higher mitotic rate in the FG roof (dorsal side) than in the floor (ventral side) at HH8, consistent with proliferation patterns of Miller et al. (1999) for HH6-8. These investigators also found a higher rate on the cranial side of the FG floor compared with the caudal side. Bellairs (1957) found similar patterns in the mesoderm, but proliferation rates were generally higher than in the endoderm. All these results are qualitatively consistent with the differential growth patterns specified in our model (Fig. 5D). In addition, a parameter study has shown that these gradients are needed to produce realistic folding morphology (Fig. S3A).

Phase 2: AIP descension

In our model, regional contraction in the endoderm during Phase 2 generates tension along and tangent to the AIP. Combined with the curvature of the AIP, this tension exerts a net downward force on the iSPL that stretches the floor of the FG and the overlying mesoderm as the AIP descends (Fig. 6, top row, Phase 2). Our blebbistatin experiments support this mechanism, as blocking contraction inhibited AIP descension during Phase 2 (Fig. 3Aa-Ad,B). Previous studies have found that contraction around the AIP also pulls pre-cardiac mesoderm towards the midline during these early stages (Varner and Taber, 2012a; Aleksandrova et al., 2015; Shi et al., 2015).

Our experiments indicate that inhibiting cell proliferation during Phase 2 slows the rate at which the AIP descends (Fig. 2C). Not surprisingly, the same behavior occurs when growth is turned off during Phase 2 in our model (Fig. 8), because AIP contraction must overcome the increasing tension that develops in the SPL as it stretches. Normally, this tension would be reduced by axial growth, which might be triggered by the increased stress (Aegerter-Wilmsen et al., 2010). These results suggest that both mechanical stretching and growth contribute to lengthening the FG.

Previous work supports this mechanism for FG elongation. Using tissue labeling techniques, Rosenquist (1966) and Stalsberg and DeHaan (1968) showed that the FG lengthens, at least in part, by

Development (2017) 144, 2381-2391 doi:10.1242/dev.145193

stretching. The latter investigators also used a mathematical model to show that the observed behavior could be caused by a force that pulls the AIP downward, and they suggested that this force is transmitted through the endoderm by notochord elongation and regression of the primitive streak. In our model, AIP contraction supplies this force. They also speculated that cell rearrangement effectively causes the FG to grow longer, reducing the build-up in tension. More recently, however, Kirby et al. (2003) obtained evidence that growth contributes to lengthening of the floor of the FG, consistent with our results.

Interestingly, exposure to aphidicolin during Phase 2 led to cardia bifida in most embryos (Fig. 2C). The reason for this is not clear, but we speculate that increased iSPL tension impedes fusion of the HFs, producing two hearts. Previous studies have found that cutting the middle of the AIP or blocking contraction between stages HH5 and HH7 can lead to cardia bifida (Varner and Taber, 2012a; Wei et al., 2001).

Phase 3: Heart tube formation

During Phase 3 in the model, cardiac jelly pressure and tissue growth separate the HFs from the endoderm and cause the HFs to expand circumferentially. As the cycle length for cells within the HT is about 5.5 days during HH9-10 (van den Berg et al., 2009), any growth is likely to be caused by cells added to the HT from a pool of highly proliferating mesodermal cells on the FG wall (van den Berg et al., 2009). These cells belong to the so-called second heart field, which later adds segments to the ends of the HT (Kirby, 2007; van den Berg et al., 2009; Abu-Issa, 2014).

Multiple processes, therefore, probably contribute to lengthening of the HT (Abu-Issa and Kirby, 2007; Kirby, 2007; van den Berg et al., 2009; Abu-Issa, 2014; Moreno-Rodriguez et al., 2006): (1) stretching driven by AIP contraction and descension (HH7-9); (2) cell influx (HH9-18); and (3) mesodermal fusion or 'zipping' (HH10-16). The role of these mechanisms and how they might interact remain subject to debate, however.

Although there are some discrepancies, the shapes of the FG, HT, OVs and AIP produced by our model agree reasonably well with actual morphology at HH10 (Fig. 7). Although the model contains some parameters that have not been clearly defined, this is not a trivial result. Nevertheless, future studies are needed to reduce the number of unknowns, as well as to confirm our main assumptions.

A parameter study shows that the fundamental behavior of the proposed model is relatively robust (Figs S3 and S4). However, the effects of cardiac jelly pressure in the model (Fig. S4B,B′) are considerably less dramatic than those observed in hyaluronidase-treated embryos (Fig. S2B,D). These results could indicate that pressure-induced wall stresses create a tension gradient that induces mesodermal cells to move into the HT (tensotaxis).

Limitations

In this study, our intent is to test the physical plausibility of our hypothesis for HT and FG formation, not to determine the molecular signals that regulate this process or the precise patterns of growth and contraction needed to produce realistic morphology. These aspects warrant future study.

To keep the problem manageable, the model geometry is relatively simple, although it includes the most essential features of the problem. For instance, during Phases 1 and 2 the model does not include the oSPL, which undergoes complex deformations during folding and, as discussed above, is likely to relax or grow considerably so it does not hinder FG formation. Thus, we do not expect this membrane to significantly affect our basic results. Including other features into the model should improve the predicted morphology.

In conclusion, the results of our study suggest that a relatively simple combination of differential growth between mesoderm and endoderm and contraction along the AIP create the FG and HT in the early chick embryo. These results are not conclusive, however, and other mechanisms might be involved. We hope that these ideas stimulate further research on this topic.

MATERIALS AND METHODS

This section describes experimental methods. Detailed computational methods are provided in supplementary Materials and Methods.

Embryo preparation and culture

Fertilized white Leghorn chicken eggs were incubated at 38°C for 20-35 h to reach stages HH5-HH10. As described in Voronov and Taber (2002), embryos were removed from the egg using a filter paper method and cultured in media consisting of 89% Dulbecco's modified Eagle's medium, 10% chick serum and 1% antibiotics.

Imaging

Brightfield images and video recordings were captured with a Nikon EOS T3 camera on a Leica DMLB MZ 8 microscope. Cross-sectional images of living embryos were acquired using a Thorlabs OCT system coupled to a Nikon FN1 microscope. Image stacks were acquired at approximately 10 µm resolution. Subsequent image analysis was performed using ImageJ.

Chemical perturbations

To inhibit cytoskeletal contraction, embryos were cultured in media containing 75 µM blebbistatin (Sigma). To inhibit cell proliferation, embryos were exposed to 50 µM aphidicolin (Santa Cruz Biotechnology), which inhibits DNA synthesis (Zagris and Matthopoulos, 1989; Firmino et al., 2016; Cui et al., 2005). Proliferation was visualized by labeling cells with EdU (see supplementary Materials and Methods for details). In selected experiments, the inhibitors were washed out by rinsing the embryo several times in PBS and then continuing the culture in normal media.

To greatly reduce cardiac jelly, embryos were cultured in media containing ovine hyaluronidase (Hyal, 20 UTR/ml; Sigma) (Baldwin and Solursh, 1989; Linask et al., 2003).

Stress estimates

To characterize stress in the FG, we used glass microneedles with circular cross-sections (outer diameter $d \approx 60$ µm) to punch holes through the oSPL, head ectoderm, and FG. Immediately after wounding, brightfield and OCT images were captured. All wounds were approximately elliptical in shape (Fig. 10A′,A″). The lengths of the minor and major axes (a and b) in the FG were measured from transverse and longitudinal OCT sections and used to compute elastic stretch ratios, $\lambda_x^* = a/d$ and $\lambda_y^* = b/d$, in the transverse and longitudinal directions, respectively (Fig. 10B,B′).

The elastic stretch ratios characterize the magnitudes of the principal stresses (Varner and Taber, 2009). The values $\lambda_i^* > 1$ and $\lambda_i^* < 1$ indicate tension and compression, respectively, in the i direction.

Measurements of tissue deformation and growth

Deformation was quantified by tracking the motions of tissue labels (microbeads) during culture. Tungsten beads (10 µm diameter) were injected into the tissue using a gene gun (Helios Gene Gun, Bio-Rad) (O'Brien et al., 2001). Brightfield images were acquired at the beginning of the experiment and approximately every 2 h during culture. Deformation rates and strains were computed from bead coordinates, and growth was estimated from strain and stress data (see supplementary Materials and Methods for more details).

Statistical analysis

Because of the nature of our study, most data analysis involves comparison of numerical and experimental results. Experimental data are plotted as

group means with error bars representing s.d. Two-way ANOVA was performed on experimental tension results using SigmaPlot (Systat Software) with $P<0.05$ considered significant.

Acknowledgements
We are grateful to Philip Bayly and Ruth Okamoto for valuable discussions. We also thank Yunfei Shi for useful suggestions regarding computational modeling in ABAQUS, as well as Alina Oltean for her advice on experiments and installation of the gene gun.

Competing interests
The authors declare no competing or financial interests.

Author contributions
Conceptualization: H.S.H., L.A.T.; Methodology: H.S.H., K.E.G., L.A.T.; Software: H.S.H.; Validation: H.S.H., K.E.G.; Formal analysis: H.S.H., L.A.T.; Investigation: H.S.H., K.E.G.; Resources: L.A.T.; Data curation: H.S.H., K.E.G.; Writing - original draft: H.S.H., K.E.G., L.A.T.; Writing - review & editing: H.S.H., K.E.G., L.A.T.; Visualization: H.S.H., K.E.G.; Supervision: L.A.T.; Project administration: L.A.T.; Funding acquisition: L.A.T.

Funding
This work was supported by grants from the National Institutes of Health [R01 NS070918 to L.A.T.; T32 EB018266 to K.E.G.]. Deposited in PMC for release after 12 months.

Supplementary information
Supplementary information available online at
http://dev.biologists.org/lookup/doi/10.1242/dev.145193.supplemental

References

Abu-Issa, R. (2014). Heart fields: spatial polarity and temporal dynamics. *Anat. Rec.* **297**, 175-182.
Abu-Issa, R. and Kirby, M. L. (2007). Heart field: from mesoderm to heart tube. *Rev. Cell Dev. Biol.* **23**, 45-68.
Abu-Issa, R. and Kirby, M. L. (2008). Patterning of the heart field in the chick. *Dev. Biol.* **319**, 223-233.
Aegerter-Wilmsen, T., Smith, A. C., Christen, A. J., Aegerter, C. M., Hafen, E. and Basler, K. (2010). Exploring the effects of mechanical feedback on epithelial topology. *Development* **137**, 499-506.
Aleksandrova, A., Czirok, A., Kosa, E., Galkin, O., Cheuvront, T. J. and Rongish, B. J. (2015). The endoderm and myocardium join forces to drive early heart tube assembly. *Dev. Biol.* **404**, 40-54.
Baldwin, H. S. and Solursh, M. (1989). Degradation of hyaluronic acid does not prevent looping of the mammalian heart in situ. *Dev. Biol.* **136**, 555-559.
Bellairs, R. (1953a). Studies on the development of the foregut in the chick blastoderm. i. the presumptive foregut area. *J. Embryol. Exp. Morphol.* **1**, 115-124.
Bellairs, R. (1953b). Studies on the development of the foregut in the chick blastoderm. ii. the morphogenetic movements. *J. Embryol. Exp. Morphol.* **1**, 369-385.
Bellairs, R. (1955). Studies on the development of the foregut in the chick iii. the role of mitosis. *J. Embryol. Exp. Morphol.* **3**, 242-250.
Bellairs, R. (1957). Studies on the development of the foregut in the chick embryo. 4. mesodermal induction and mitosis. *J. Embryol. Exp. Morphol.* **5**, 340-350.
Cui, C., Yang, X., Chuai, M., Glazier, J. A. and Weijer, C. J. (2005). Analysis of tissue flow patterns during primitive streak formation in the chick embryo. *Dev. Biol.* **284**, 37-47.
Cui, C., Cheuvront, T. J., Lansford, R. D., Moreno-Rodriguez, R. A., Schultheiss, T. M. and Rongish, B. J. (2009). Dynamic positional fate map of the primary heart-forming region. *Dev. Biol.* **332**, 212-222.
Davies, J. (2005). *Mechanisms of Morphogenesis: The Creation of Biological Form*. San Diego: Elsevier Academic Press.
De Jong, F., Geerts, W. J. C., Lamers, W. H., Los, J. A. and Moorman, A. F. M. (1990). Isomyosin expression pattern during formation of the tubular chicken heart: a three-dimensional immunohistochemical analysis. *Anat. Rec.* **226**, 213-227.
DeHaan, R. L. (1963). Migration patterns of the precardiac mesoderm in the early chick embryo. *Exp. Cell Res.* **29**, 544-560.
Filas, B. A., Oltean, A., Majidi, S., Bayly, P. V., Beebe, D. C. and Taber, L. A. (2012). Regional differences in actomyosin contraction shape the primary vesicles in the embryonic chicken brain. *Phys. Biol.* **9**, 066007.
Firmino, J., Rocancourt, D., Saadaoui, M., Moreau, C. and Gros, J. (2016). Cell division drives epithelial cell rearrangements during gastrulation in chick. *Dev. Cell* **36**, 249-261.
Földes, G., Mioulane, M., Wright, J. S., Liu, A. Q., Novak, P., Merkely, B., Gorelik, J., Schneider, M. D., Ali, N. N. and Harding, S. E. (2011). Modulation of human embryonic stem cell-derived cardiomyocyte growth: a testbed for studying human cardiac hypertrophy? *J. Mol. Cell. Cardiol.* **50**, 367-375.
Hamburger, V. and Hamilton, H. L. (1951). A series of normal stages in the development of the chick embryo. *J. Morphol.* **88**, 49-92.
Kirby, M. L. (2007). *Cardiac Development*. New York: Oxford University Press.
Kirby, M. L., Lawson, A., Stadt, H. A., Kumiski, D. H., Wallis, K. T., McCraney, E., Waldo, K. L., Li, Y.-X. and Schoenwolf, G. C. (2003). Hensen's node gives rise to the ventral midline of the foregut: Implications for organizing head and heart development. *Dev. Biol.* **253**, 175-188.
Koehl, M. A. R., Quillin, K. J. and Pell, C. A. (2000). Mechanical design of fiber-wound hydraulic skeletons: The stiffening and straightening of embryonic notochords. *Am. Zool.* **40**, 28-41.
Li, F., Wang, X., Bunger, P. C. and Gerdes, A. M. (1997). Formation of binucleated cardiac myocytes in rat heart: I. Role of actin-myosin contractile ring. *J. Mol. Cell. Cardiol.* **29**, 1541-1551.
Linask, K. K. and Lash, J. W. (1986). Precardiac cell migration: fibronectin localization at mesodermendoderm interface during directional movement. *Dev. Biol.* **114**, 87-101.
Linask, K. K., Han, M.-D., Linask, K. L., Schlange, T. and Brand, T. (2003). Effects of antisense misexpression of cfc on downstream flectin protein expression during heart looping. *Dev. Dyn.* **228**, 217-230.
Manasek, F., Isobe, Y., Shimada, Y., Hopkins, W., Nora, J. and Takao, A. (1984). The embryonic myocardial cytoskeleton, interstitial pressure, and the control of morphogenesis. In *Congenital Heart Disease: Causes and Processes* (ed. J. J. Nora and A. Takeo), pp. 359-376. New York: Futura Publishing.
Männer, J. (2000). Cardiac looping in the chick embryo: a morphological review with special reference to terminological and biomechanical aspects of the looping process. *Anat. Rec.* **259**, 248-262.
Miller, S. A., Adornato, M., Briglin, A., Cavanaugh, M., Christian, T., Jewett, K., Michaelson, C., Monoson, T., Price, F., Tignor, J. et al. (1999). Domains of differential cell proliferation suggest hinged folding in avian gut endoderm. *Dev. Dyn.* **216**, 398-410.
Moreno-Rodriguez, R. A., Krug, E. L., Reyes, L., Villavicencio, L., Mjaatvedt, C. H. and Markwald, R. R. (2006). Bidirectional fusion of the heart-forming fields in the developing chick embryo. *Dev. Dyn.* **235**, 191-202.
Nakamura, A. and Manasek, F. (1978). Experimental studies of the shape and structure of isolated cardiac jelly. *J. Embryol. Exp. Morphol.* **43**, 167-118.
Nakamura, A. and Manasek, F. (1981). An experimental study of the relation of cardiac jelly to the shape of the early chick embryonic heart. *J. Embryol. Exp. Morphol.* **65**, 235-256.
O'Brien, J. A., Holt, M., Whiteside, G., Lummis, S. C. R. and Hastings, M. H. (2001). Modifications to the hand-held gene gun: improvements for in vitro biolistic transfection of organotypic neuronal tissue. *J. Neurosci. Methods* **112**, 57-64.
Olson, E. N. and Srivastava, D. (2002). Molecular pathways controlling heart development. *Science* **272**, 671-676.
Patten, B. M. (1951). *Early Embryology of the Chick*. New York: McGraw-Hill.
Ramasubramanian, A., Latacha, K. S., Benjamin, J. M., Voronov, D. A., Ravi, A. and Taber, L. A. (2006). Computational model for early cardiac looping. *Ann. Biomed. Eng.* **34**, 1355-1369.
Rodriguez, E. K., Hoger, A. and McCulloch, A. D. (1994). Stress-dependent finite growth in soft elastic tissues. *J. Biomech.* **27**, 455-467.
Romanoff, A. (1960). *The Avian Embryo: Structural and Functional Development*. New York: Macmillan.
Rosenquist, G. (1966). *A Radioautographic Study of Labeled Grafts in the Chick Blastoderm: Development from Primitive-Streak Stages to Stage 12*. Washington DC, USA: Carnegie Institution of Washington.
Schultheiss, T. M., Xydas, S. and Lassar, A. B. (1995). Induction of avian cardiac myogenesis by anterior endoderm. *Development* **121**, 4203-4214.
Shi, Y., Yao, J., Xu, G., Perucchio, R. and Taber, L. A. (2014). Bending of the looping heart: differential growth revisited. *J. Biomech. Eng.* **5**, 297.
Shi, Y., Varner, V. D. and Taber, L. A. (2015). Why is cytoskeletal contraction required for cardiac fusion before but not after looping begins? *Phys. Biol.* **12**, 016012.
Stalsberg, H. and DeHaan, R. L. (1968). Endodermal movements during foregut formation in the chick embryo. *Dev. Biol.* **18**, 198-215.
Stalsberg, H. and DeHaan, R. L. (1969). The precardiac areas and formation of the tubular heart in the chick embryo. *Dev. Biol.* **19**, 128-159.
Taber, L. A. (2004). *Nonlinear Theory of Elasticity: Applications in Biomechanics*. NJ: World Scientific Publishing Co.
Taber, L. A. (2009). Towards a unified theory for morphomechanics. *Philos. Trans. R. Soc. A Math. Phys. Eng. Sci.* **367**, 3555-3583.
Taber, L. A. (2014). Morphomechanics: transforming tubes into organs. *Curr. Opin. Genet. Dev.* **27**, 7-13.
Taber, L. A., Sun, H., Clark, E. B. and Keller, B. B. (1994). Epicardial strains in embryonic chick ventricle at stages 16 through 24. *Circ. Res.* **75**, 896-903.
van den Berg, G., Abu-Issa, R., de Boer, B. A., Hutson, M. R., de Boer, P. A. J., Soufan, A. T., Ruijter, J. M., Kirby, M. L., van den Hoff, M. J. B. and Moorman, A. F. M. (2009). A caudal proliferating growth center contributes to both poles of the forming heart tube. *Circ. Res.* **104**, 179-188.

Development (2017) 144, 2381-2391 doi:10.1242/dev.145193

Varner, V. D. and Taber, L. A. (2009). On measuring stress distributions in epithelia. *IUTAM Symp. Cell. Mol. Tissue Mech.* **16**, 45-54.

Varner, V. D. and Taber, L. A. (2012a). Not just inductive: a crucial mechanical role for the endoderm during heart tube assembly. *Development* **139**, 1680-1690.

Varner, V. D. and Taber, L. A. (2012b). On integrating experimental and theoretical models to determine physical mechanisms of morphogenesis. *Biosystems* **109**, 412-419.

Varner, V. D., Voronov, D. A. and Taber, L. A. (2010). Mechanics of head fold formation: Investigating tissue-level forces during early development. *Development* **137**, 3801-3811.

Voronov, D. A. and Taber, L. A. (2002). Cardiac looping in experimental conditions: effects of extra embryonic forces. *Dev. Dyn.* **224**, 413-421.

Voronov, D. A., Alford, P. W., Xu, G. and Taber, L. A. (2004). The role of mechanical forces in dextral rotation during cardiac looping in the chick embryo. *Dev. Biol.* **272**, 339-350.

Warren, M., Puskarczyk, K. and Chapman, S. C. (2009). Chick embryo proliferation studies using edu labeling. *Dev. Dyn.* **238**, 944-949.

Wei, L., Roberts, W., Wang, L., Yamada, M., Zhang, S., Zhao, Z., Rivkees, S., Schwartz, R. and Imanaka-Yoshida, K. (2001). Rho kinases play an obligatory role in vertebrate embryonic organogenesis. *Development* **128**, 2953-2962.

Young, J. M., Yao, J., Ramasubramanian, A., Taber, L. A. and Perucchio, R. (2010). Automatic generation of user material subroutines for biomechanical growth analysis. *ASME J. Biomech. Eng.* **132**, 104505.

Yutzey, K. E. and Kirby, M. L. (2002). Wherefore heart thou? embryonic origins of cardiogenic mesoderm. *Dev. Dyn.* **223**, 307-320.

Zagris, N. and Matthopoulos, D. (1989). Stage-specific gene expression in early chick embryo. *Dev. Genet.* **10**, 333-338.

Zamir, E. A. and Taber, L. A. (2004). Material properties and residual stress in the stage 12 chick heart during cardiac looping. *J. Biomech. Eng.* **126**, 823-830.